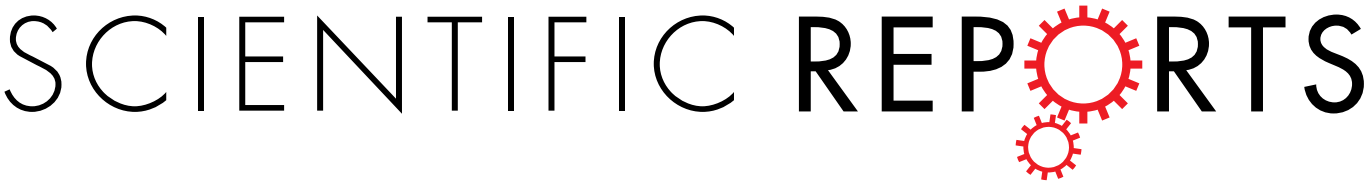

OPEN

# Highly Performance Core-Shell $TiO_2$(B)/anatase Homojunction Nanobelts with Active Cobalt phosphide Cocatalyst for Hydrogen Production

Received: 30 August 2017
Accepted: 20 October 2017
Published online: 06 November 2017

Guang Yang, Hao Ding, Jiejie Feng, Qiang Hao, Sijia Sun, Weihua Ao & Daimei Chen

**In this paper, a highly efficient core-shell structure of $TiO_2$(B)/anatase photocatalyst with CoP cocatalyst has been synthesized via hydrothermal processes and a mechanical milling method. The designed core-shell $TiO_2$(B)/anatase photocatalysts exhibit excellent performance by compared with pure $TiO_2$(B) and anatase phase. With the participation of CoP particles, there is drastically enhanced photocatalytic activity of $TiO_2$(B)/anatase, and the $H_2$-production rate can be up to 7400 $\mu mol \cdot g^{-1}$, which is about 3.2 times higher than $TiO_2$(B)/anatase photocatalyst. The improved activity is attributed to the contribution of the well-matched core-shell structure and cooperative effect of CoP cocatalyst. The photogenerated holes of anatase can migrate more promptly to the adjacent $TiO_2$(B) core than the photogenerated electrons, which result in an accumulation of electrons in the anatase, and CoP nanoparticles can contribute significantly to transferring electrons from the surface of $TiO_2$(A). It was found that the efficient separation of electron-hole pairs greatly improved the photocatalytic hydrogen evolution in water under UV light irradiation.**

Photocatalytic hydrogen production from water using solar energy has received increasing attention because this strategy is considered to be a globally accepted way for solving the energy problem[1–7]. Titanium dioxide ($TiO_2$), especially anatase phase photocatalysts, has attracted significant attention in photocatalytic hydrogen evolution due to its low cost, excellent chemical stability and superior photocatalytic activity[8,9]. Nevertheless, $TiO_2$ can only be motivated by UV-light due to its large band gap (3.2 eV), and the fast recombination of photogenerated electrons and holes limits the application of $TiO_2$. Therefore, many researchers focus on $TiO_2$ to make it sensitive to visible light and to inhibit the recombination of photogenerated charge carrier, which affect its overall photocatalytic efficiency.

Construction of homojunction photocatalysts might be a common and effective way to improve the separation efficiency of photoinduced electron-hole pairs. The commercially available photocatalysts, such as Degussa P25 $TiO_2$, has been found to exhibit a better photoactivity than pure anatase in many reaction systems. The efficient electron and holes transferring between the two phases can increase lifetime of electrons and holes[10–13]. Coincidentally, a relatively new $TiO_2$(B) crystal phase is observed, which shows different crystal structures with anatase, rutile, and brookite. Although the photocatalytic efficiency of $TiO_2$ (B) is lower than anatase, the former phase possesses a narrow bandgap and specific conduction band (CB) and valence band (VB) edge potential. Thus, the potential difference between the CB and VB edges of the two phases can promote charge transfer from one phase to the other when $TiO_2$(B) and anatase combined with each other forming a homojunction[14]. Li *et al.* synthesized core-shell anatase/$TiO_2$(B) nanofiber, which shows enhanced photocatalytic activity compared to either single-crystal anatase or single-crystal $TiO_2$(B) nanofiber[15]. Li's group synthesized $TiO_2$(B)-anatase

Beijing Key Laboratory of Materials Utilization of Nonmetallic Minerals and Solid Wastes, National Laboratory of Mineral Materials, School of Materials Science and Technology, China University of Geosciences, Xueyuan Road, Haidian District, Beijing, 100083, P.R. China. Correspondence and requests for materials should be addressed to H.D. (email: dinghao113@126.com) or D.C. (email: chendaimei@cugb.edu.cn)

homojunction with disordered surface shell, and the excellent performance for photocatalytic hydrogen evolution was 580 μmol $h^{-1}$ under simulated solar light irradiation (0.02 g photocatalyst)[16].

Although homojunction can improve the charge transfer, the $H_2$-production efficiency of $TiO_2$(B)/anatase is still limited because the accumulated electrons in CB may recombine with the holes in VB easily. So, it is a wide and effective strategy to load proper oxidation or reduction cocatalysts on the surface of semiconductor photocatalysts[17–19]. Various kinds of cocatalysts have been applied to $TiO_2$ photocatalysts to improve the activity of $H_2$ evolution reactions, including metal cocatalysts, metal oxide/sulfide cocatalysts and noble metals (e.g. Pt, Ag, Au and Ru)[20–25]. However, the preparation of these cocatalysts particles is complicated and quite expensive for widespread practical application. A variety of non-precious cocatalysts have been reported, including MoS[26], Cu(OH)[27], NiS[28], NiO[29]. Recently, transition metal phosphides, including $Ni_2P$, CoP, FeP, MoP and $Cu_3P$ have been exploited in electrocatalysis of the hydrogen evolution reaction, and achieved outstanding efficiency[30–32]. During these pioneering works, it has been noticed that CoP nanoparticles show good electrical conductivity with metallic behavior. Chen's group discovered that CoP nanoparticles together with CdS nanorods exhibited excellent efficiency for photocatalytic hydrogen evolution[33,34]. We envision that the hydrogen production performance can be dramatically improved by choosing CoP cocatalysts nanoparticles.

Herein, we designed $TiO_2$(B)/anatase core-shell homojunction nanobelts using CoP nanoparticles as cocatalysts for efficient photocatalytic $H_2$ production from aqueous methanol solution. The electrons migrate to the same destinations are times longer than holes in $TiO_2$(B)/anatase system, and the accumulated electrons can be easily separate and transfer with the participation of CoP cocatalyst. The subsequently photocatalytic $H_2$-production reduction reactions can be effectively enhanced. So, it is believed that this strategy is feasible and will have great practical application for hydrogen production.

## Experimental

**Synthesis of core-shell structure photocatalyst.** Core-Shell $TiO_2$ nanobelts were obtained using a previously reported procedure[35]. 3 g of anatase powder was mixed with 40 mL of 10 M NaOH solution. The suspension were dispersed in an ultrasonic bath for 30 min then transferred into into a Teflon-lined stainless steel autoclave, sealed and maintained at the temperature of 180 °C for 48 h. The precipitate (sodium titanate nanobelts) was collected, washed with distilled water several times to remove excess NaOH. Then, the obtained precursor was exchanged with $H^+$ using a 0.1 M HCl solution for 24 h to form $H_2Ti_3O_7$ nanofibers. The product washed again with distilled water to neutral and dried at 70 °C for 10 h. The core-shell photocatalyst was synthesized by hydrothermal treatment of precursors in an acid environment and further subjected to heating process. 0.8 g of $H_2Ti_3O_7$ nanofibers were dispersed in a dilute (0.05 M, 80 mL) $HNO_3$ acid solution and kept at 110 °C for 48 h. The dried powder was heated in a muffle oven at 450 °C (2 °C/min) in air for 4 h, named T (AB). Reference samples: (1) Anatase catalyst was prepared by prolonging the hydrothermal reaction ($HNO_3$ acid solution) time to 60 h and calcining at 450 °C in air for 4 h, noted as T (A); (2) $TiO_2$ (B) catalyst was obtained by using dried $H_2Ti_3O_7$ powder heated at 450 °C for 4 h, noted as T (B).

**Synthesis of CoP nanoparticles.** CoP nanoparticles were prepared via a thermal phosphidation reaction using $Co(OH)_2$ as precursor[33]. 200 mg of $Co(NO_3)_2{\cdot}6H_2O$ was added to 100 mL aqueous solution containing 50 mg sodium citrate and stirred for 15 min. Then excess NaOH solution (0.5 M) was added to the mixture dropwise. The formed Co $(OH)_2$ suspension was separated by centrifugation and dried at vacuum oven. Afterwards, 50 mg of obtained Co $(OH)_2$ and 250 mg $NaH_2PO_2$ solid were ground in a mortar to form a uniform distribution and put in a quartz boat. Subsequently, the samples were maintained in tube furnace at 300 °C for 1 h with a heating rate of 2 °C·$min^{-1}$ in a flowing Ar atmosphere (30 mL/min). Following cooling to room temperature, the obtained black solid was washed subsequently by water and ethanol three times and dried at vacuum oven.

**Loading of CoP Cocatalyst.** The loading of CoP nanoparticles on $TiO_2$(B)/anatase core-shell photocatalyst was conducted by a mechanical milling method, the preparation process as shown in Fig. 1.

**Characterizations.** X-ray diffraction (XRD) datas of the as-synthesized samples were recorded by a Brukeer D8A A25X X-ray diffractometer system using Cu Kα (λ = 0.15406 nm) radiation. The morphologies of the prepared samples were performed using a Hitachi SU-8010 instrument. High-resolution transmission electron microscopy (HR-TEM) and energy-dispersive X-ray spectroscopy (EDS) were applied to investigate the microstructure using a Tecnai $G^2$ F30 instrument (HR-TEM operated at 200 kV). The UV-vis diffuse reflectance (DR) spectra of the samples were tested on a Hitachi U-3010 double beam spectrophotometer. The photoluminescence (PL) spectra were measured on a high-resolution multi-function imaging spectrometer (iHR 550) using laser transmitter (532 nm). X-ray photoelectron spectroscopy (XPS) was performed on an K-Alpha spectrometer (THERMO FISHERSCIENTIFIC).

**Photocatalytic $H_2$-production.** The photocatalytic $H_2$-production experiment was carried out as follows, 100 mg photocatalyst and 10 mL methanol were added into the tube. Then the total volume of the mixed solution was adjusted to 100 mL with distilled water. A 300 W Xe lamp was used as light source and the electric current recorded to be 15A. Before light irradiation, the gas-tight system kept for several hours to make sure the tightness of all system and adsorption-desorption equilibrium between the photocatalyst and gases. The gas products were periodically analyzed by using a gas chromatography (GC-2014, Shimadzu Corp, Japan), which was equipped with a 5 Å molecular sieve column (3 m × 2 mm).

## Results and Discussion

Figure 2 shows the XRD patterns of the as-prepared $TiO_2$(A), $TiO_2$(AB) and $TiO_2$(B) nanobelts. The obtained $TiO_2$(A) and $TiO_2$(B) samples are matched well with the crystal structure data of anatase phase (JCPDS No. 21–1272) and $TiO_2$(B) phase (JCPDS No. 46–1238)[36,37]. The peak of $TiO_2$(B) in the core-shell structure is not

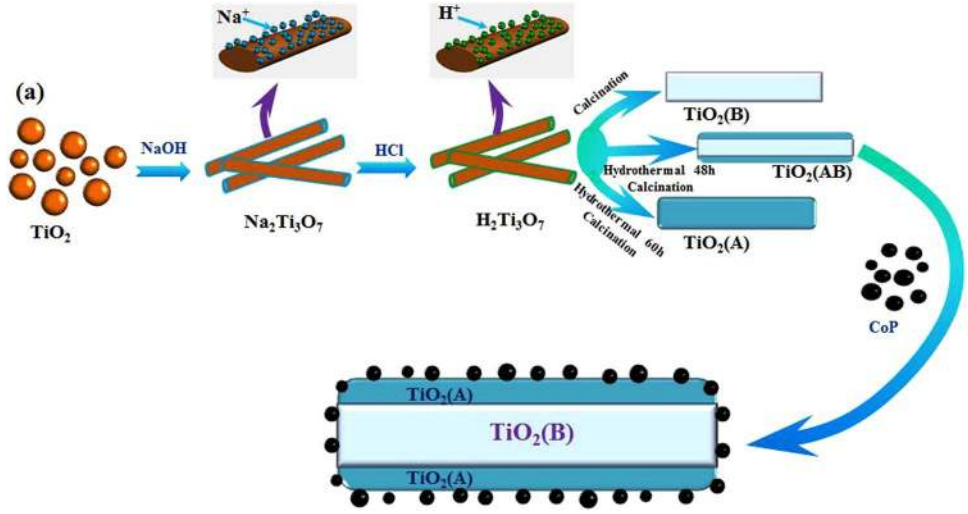


**Figure 1.** The preparation process of core-shell structure CoP/$TiO_2$(AB) photocatalyst.

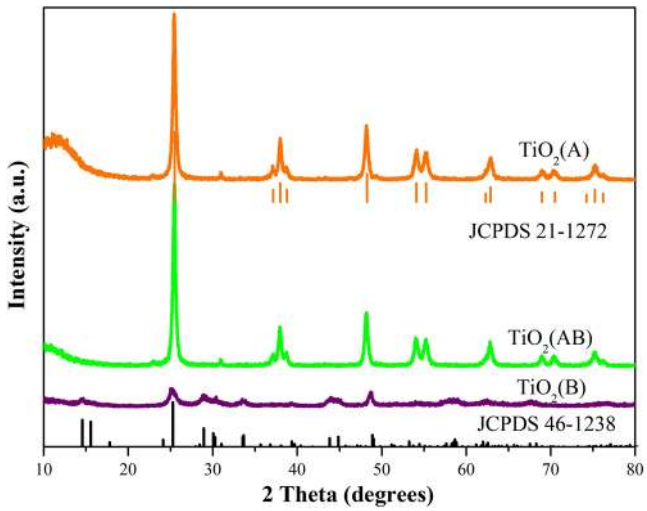


**Figure 2.** XRD patterns of $TiO_2$(B), $TiO_2$(A) and $TiO_2$(AB) phase.

obvious may attribute to the overlapped main peak between $TiO_2$(B) and $TiO_2$(A), or the low contents of $TiO_2$(B) for detection. In addition, as depicted in Figure S1, the XRD diffraction peaks of CoP nanoparticles are indistinguishable for each sample from CoP(0.5%)/$TiO_2$ to CoP(5%)/$TiO_2$ due to the low loading amount and weak crystallization of CoP nanoparticle. Similar phenomenon has been observed for other photocatalysts[33,38].

The scanning electron microscopy (SEM) characterization can provide the direct evidence for the coexistence of CoP and $TiO_2$. It can be seen that CoP nanoparticles are polydisperse (Figure S2a) and $TiO_2$(AB) are nanobelts-like morphologies (Figure S2b). After coating with CoP nanoparticles, Co and P elements are distributed well on the surface of $TiO_2$(AB) nanobelts photocatalyst (Figure S2c,d). The CoP-$TiO_2$(AB) composites structure can be further confirmed in the EDS mappings analysis presented in Figure S2e. The results indicate that the Co, P, Ti and O elemental are uniformly distributed, and no other elements are detected. Furthermore, the corresponding energy dispersive X-ray spectroscopy (EDX) analysis confirms the existence of CoP and $TiO_2$. However, the content of the measured CoP is lower than theoretical values in the final composites because of only surface CoP atoms can be checked (see Supplementary Figure S3).

To investigate the existence of core-shell homojunction, more explicit structure evolution is shown in transmission electron microscopy (TEM). As described in Fig. 3a, the typical $TiO_2$(B)/anatase core-shell nanobelts can be observed clearly. The core of the nanobelts is corresponding to $TiO_2$(B) phase, while the shell conforms to anatase phase. The HRTEM confirms that the sample possesses a homojunction structure with well-matched lattice fringes of the (110) plane of $TiO_2$(B) and (101) plane of anatase (Fig. 3b). The TEM images of CoP(1%)-$TiO_2$(AB) sample as depicted in Fig. 3c clearly indicate CoP nanoparticles (the red circle) are deposited on the surface of $TiO_2$(AB) photocatalyst. The HRTEM image further shows that $TiO_2$(AB) and CoP nanoparticles are in close contact with each other (Fig. 3d). The lattice spacings of ca. 0.35 nm and 0.19 nm belong to the diffraction planes of $TiO_2$(A) and CoP nanoparticles, respectively.

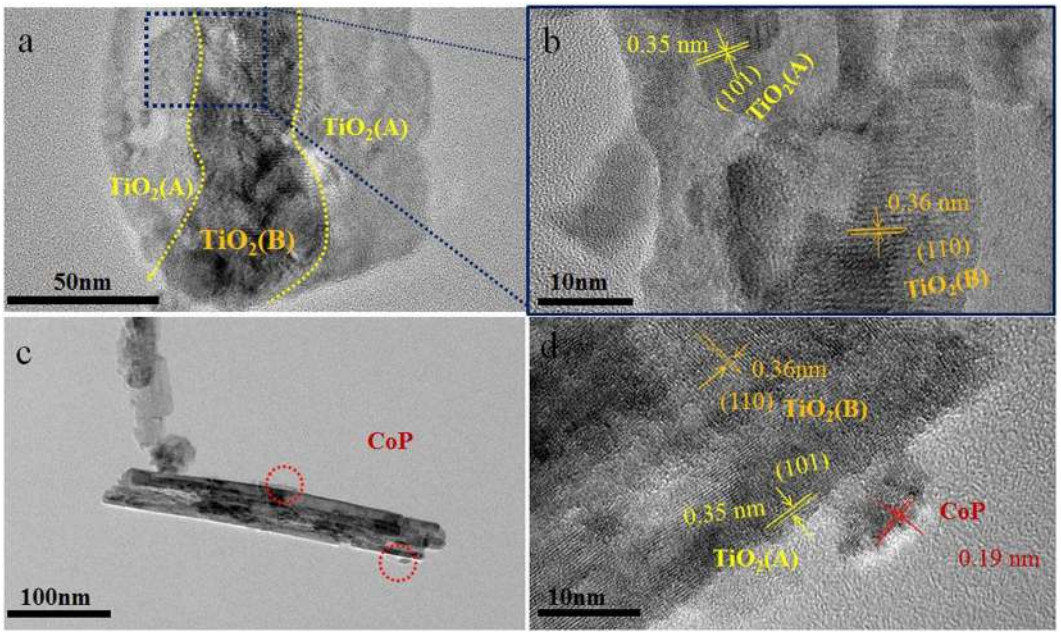


**Figure 3.** (**a**,**b**) TEM images of $TiO_2$(AB) photocatalysts; (**c**,**d**) TEM and HRTEM image of CoP(1%)-$TiO_2$(AB) photocatalysts.

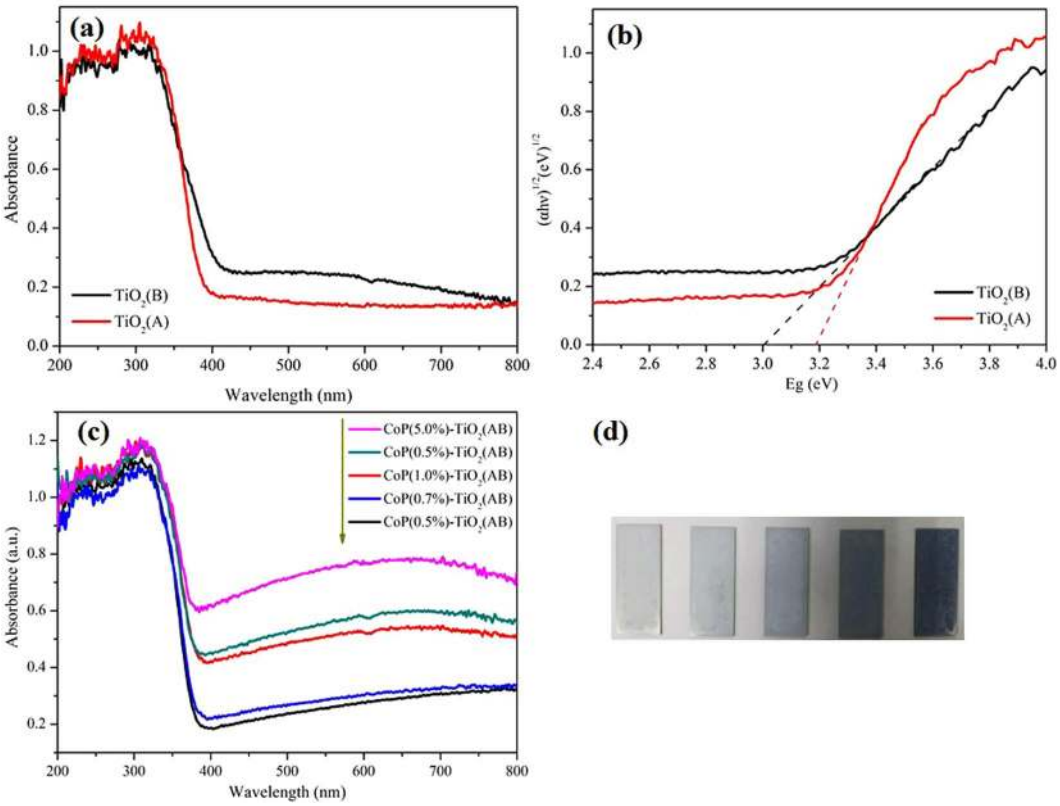


**Figure 4.** (**a**) UV-Vis DRS and (**b**) The plots of between $(\alpha h\upsilon)^{1/2}$ and Eg for $TiO_2$(A) and $TiO_2$(B); (**c**) UV-Vis DRS of the CoP-$TiO_2$ composites; (**d**) The optical photograph of the composite samples with different CoP content.

The optical properties of the $TiO_2$(B) and $TiO_2$(A) are investigated by UV-Vis diffuse reflectance spectra (DRS) as given in Fig. 4a. The absorption edges of pure $TiO_2$(B) and $TiO_2$(A) are 406 nm and 388 nm, respectively. According to Tauc formula $[\alpha h\nu = A(h\nu - Eg)^{n/2}]$, the band gaps of $TiO_2$(B) and $TiO_2$(A) are estimated to be

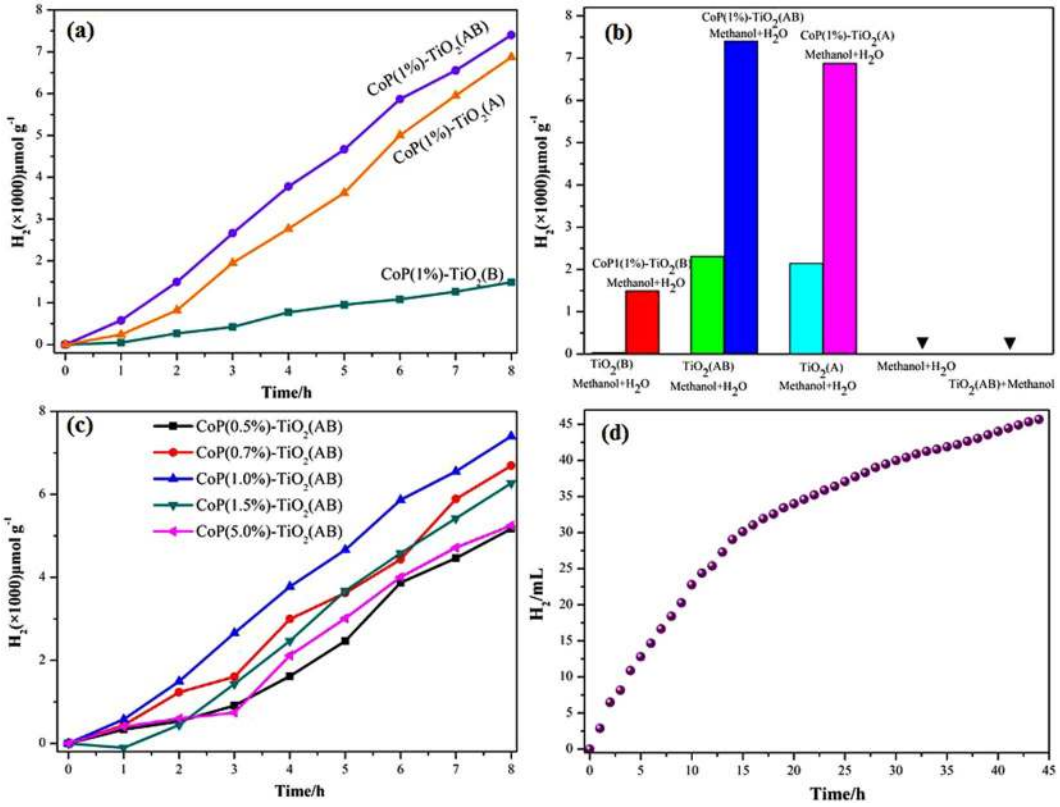


**Figure 5.** (**a**) The $H_2$ generation rates of $TiO_2$(A), $TiO_2$(B) and $TiO_2$(AB) with 1%CoP cocatalyst; (**b**) Activity comparisons between different $TiO_2$ phase and CoP/$TiO_2$ photocatalysts (**c**) Photocatalytic activities of CoP/$TiO_2$(AB) hybrid photocatalysts with different CoP contents; (**d**) Photocatalytic durability test for CoP/$TiO_2$(AB).

3.05 and 3.19 eV, respectively (Fig. 4b). With the increasing loading of CoP, a red-shift DRS of is observed in the CoP-$TiO_2$(AB) composite materials, which can be attributed to the absorption of CoP nanoparticles (Fig. 4c). However, there is no significant absorption edge change of the CoP-$TiO_2$(AB) samples, indicating that CoP is incorporated onto the surface of $TiO_2$(AB) rather than into the lattice[34]. Besides, the color of the composite photocatalyst becomes brown due to the absorption of CoP particles. The XPS spectrum results of $TiO_2$(B), $TiO_2$(AB), $TiO_2$(A) and CoP are presented in Figure S4. The high resolution XPS spectrum shows O1s, Ti2p, P2p and Co2p, respectively. The binding energy of as-fabricated $TiO_2$(B), $TiO_2$(AB) and $TiO_2$(A) is not changed for both Ti2p and O1s. In addition, the binding energy peaks of P 2p and Co (2p3/2) are in agreement with the reported ones[33]. Compared with $TiO_2$(AB) (35.4 $m^2 g^{-1}$) sample, the as-prepared CoP(1%)-$TiO_2$(AB) composite sample shows a small specific surface area of 30.53 $m^2 g^{-1}$ (Figure S5).

The photocatalytic performances of the as-prepared $TiO_2$(A), $TiO_2$(B) and $TiO_2$(AB) samples are monitored for hydrogen production evolution from pure water containing methanol as sacrificial reagents under simulated sunlight irradiation. As plotted in Fig. 5a, it clearly seen that the core-shell structure $TiO_2$(AB) catalysts express the highest yield of $H_2$ with loading of 1% CoP cocatalysts. In the absence of cocatalysts, a sharp decrease of $H_2$ production is observed for $TiO_2$(A), $TiO_2$(B) and $TiO_2$(AB) samples. The highest $H_2$-production rate of CoP(1%)- $TiO_2$(AB) can be up to 7400 μmol $g^{-1}$, which is about 3.2-times higher than that of $TiO_2$(AB) (2306 μmol $g^{-1}$) (Fig. 5b). The notably performance imply that CoP is an effective cocatalyst, which show impact on enhancing the photocatalytic activity positive. To check whether $H_2$ produced is from water or methanol, blank experiments without catalysts is conducted. There is no $H_2$ generation that suggested water is probably the real substrate in the photocatalytic reaction, and the conclusion is also verified by other authors[33,39]. The photocatalytic activity of the core-shell structure $TiO_2$(AB) photocatalysts with different mount of CoP cocatalysts are also studied (Fig. 5c). As the amount of CoP increases, the $H_2$ evolution rate is further enhanced, reaching the maximum value for CoP(1%)-$TiO_2$. However, there is a decrease in the photocatalytic $H_2$ evolution with further increase the loading amount of CoP particles. Hence, the optimal loading of CoP should be 1 wt%. The results may due to the following causes: (i) with the loading dosage of CoP cocatalysts, more active sites can be provided for reduction reactions; (ii) excessive CoP nanoparticles covered on the surface $TiO_2$(AB) or aggregated into larger nanoparticles shielding surface active sites, which may lead to a negative impact on their catalytic activity. This phenomenon is similar to other nanoparticle cocatalysts[40–42]. Figure 5d displays the durability of the photocatalysts after 50 hours irradiation, and the result indicate that a slight increase is measured with CoP cocatalyst. XRD patterns further demonstrate the stable of the as-prepared photocatalyst (Figure S6).

To further understand the enhancement of photocatalytic activity between Cop nanoparticles and $TiO_2$(AB) photocatalysts, transient photocurrent response and electrochemical impedance spectroscopy (EIS) are conducted under

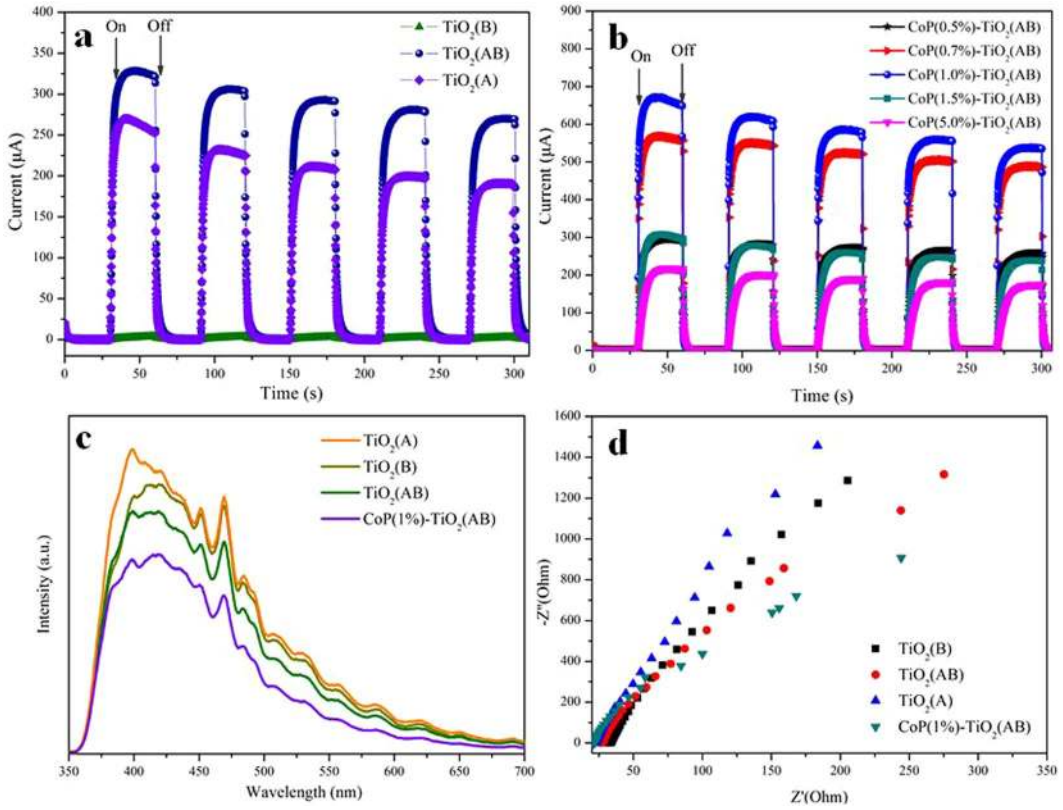


**Figure 6.** (**a**) Photogenerated currents density of the CoP(x%)-$TiO_2$ photocatalysts and (**b**) different $TiO_2$ phase under UV-visible light; (**c**) Photoluminescence (PL) spectra and (**d**) Nyquist impedance plots of $TiO_2$(A), $TiO_2$(B), $TiO_2$(AB) and CoP(1%)-$TiO_2$(AB) samples.

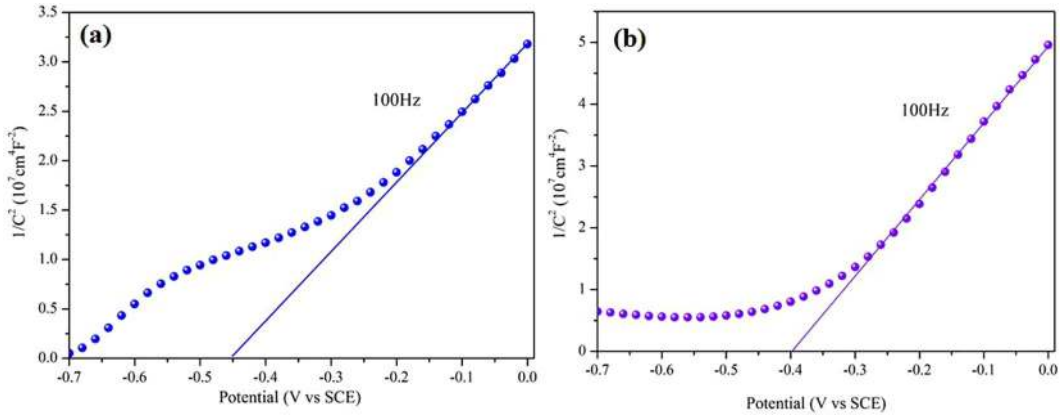


**Figure 7.** Mott-Schottky plot for (**a**) $TiO_2$(A) and (**b**) $TiO_2$(B) electrode in saturated $Na_2SO_4$ electrolyte solution (0.1 M, pH = 6.8) vs SCE.

UV-visible light irradiation. Upon illumination, the photocurrent immediately rises and the photocurrent rapidly decreases to zero as long as the light is switched off. As presented in Fig. 6a, the pulsed photocurrent density of the CoP(1%)-$TiO_2$(AB) sample is higher than other photocatalysts, suggesting more efficient separation of photoexcited electron-hole pairs happened. In addition, CoP cocatalysts exhibit improved photocurrents (650 μA) compared with pure $TiO_2$(AB) (Fig. 6b). It is notable that the change tendency agrees well with the photocatalytic $H_2$ production activity. From the photoluminescence (PL) spectra in Fig. 6c, it can be seen that the emission intensity of the samples decreases in the following order: $TiO_2$(A) < $TiO_2$(B) < $TiO_2$(AB) < CoP(1%)-$TiO_2$(AB), indicating that charge recombination can be better suppressed after loading CoP cocatalysts. The PL emission bands at around 410 nm are observed in all samples, which belong to the emission of the band gap transition of $TiO_2$[43]. Furthermore, the impedance radius of CoP(1%)-$TiO_2$(AB) is smaller than $TiO_2$(AB) (Fig. 6d), indicating that CoP can enhance separation efficiency of the photogenerated charges and facilitate the interfacial charge transfer.

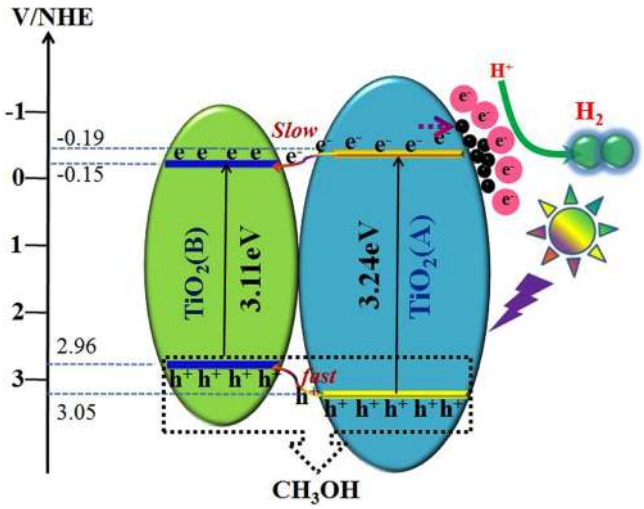


**Figure 8.** Proposed electron transfer and photocatalytic activity enhanced mechanism of CoP/$TiO_2$(AB) upon UV-visible light irradiation.

## Mechanism of CoP-$TiO_2$(AB)

In order to investigate the transfer mechanism of electrons ($e^-$) and holes ($h^+$) between $TiO_2$(A) and $TiO_2$(B), the band edge positions of conduction band (CB) and valence band (VB) of the two semiconductor are measured by Mott-Schottky measurement, which can directly probe the energy positions of $TiO_2$(A) and $TiO_2$(B). From Fig. 7, the CB and VB edges of $TiO_2$(A) nanobelts are found to be −0.19 eV and +3.05 eV (vs. NHE), and the CB and VB edges of $TiO_2$(B) nanosheets are −0.15 eV and +2.96 eV (vs. NHE), respectively. The calculation will be essential for the verification as shown in Support Information (Table 1) and early reports[35,43,44]. Accordingly, schematic diagram of the role of cocatalysts played in the separation and transfer of photogenerated charges of $TiO_2$(AB) core-shell homojunction is shown in Fig. 8. Based on the energy structure of the interface between $TiO_2$(A) and $TiO_2$(B), the photoinduced holes of $TiO_2$(A) could directly be injected into the VB of $TiO_2$(B). Meanwhile, the excited electrons in $TiO_2$(A) could be transferred to the CB of $TiO_2$(B) easily under the irradiation of UV light. In the transfer process, the early literature has verified that the photogenerated holes can migrate more promptly to the adjacent $TiO_2$(B) phase than the photogenerated electrons. Because the electrons migrate to the same destination in the same anatase crystals are 40 times longer (>40–160 ps) than those for holes (1–4 ps), which result in an accumulation of holes in the $TiO_2$(B)[35]. These photoinduced holes at the VB of $TiO_2$(A) and $TiO_2$(B) can react with the $H_2O$ to generate some oxidation groups such as hydroxyl radicals, causing the oxidation reaction with the sacrificial reagent employed such as $CH_3OH$. The overall outcome of the interphase charge migration is that a higher electron concentration left within the anatase shell. With the help of CoP cocatalyst, the photogenerated electrons on the CB of $TiO_2$(A) tend to transfer to the loaded CoP nanoparticles, which are capable of the reduction reaction. As a consequence, the loaded cocatalysts are very helpful to the separation and transfer of photogenerated electron-hole pairs. Hence, the coherent interface between anatase and $TiO_2$(B) structure and the CoP cocatalyst in the photocatalysis process may reduce recombination of photogenerated electron-hole pairs in the photocatalytic reaction and the photocatalytic activity is enhanced.

## Conclusion

In summary, a highly efficient core-shell $TiO_2$(B)/anatase photocatalyst has been fabricated successfully for photocatalytic $H_2$ evolution. The designed homojunction photocatalysts exhibited excellent performance compared with the pure phase, and a drastically enhanced photocatalytic activity appears with the participation of CoP cocatalysts. The $H_2$-production rate of CoP(1%)-$TiO_2$(AB) photocatalysts can be up to 7400 $\mu mol \cdot g^{-1}$. The remarkable activity is attributed to the cooperative contribution of effective core/shell structure that leading to the separation of photogenerated charges and the function of CoP cocatalysts on the transfer of photogenerated electrons from anatase to outside driven by the cocatalysts. This work demonstrated the great feasibility of utilizing CoP cocatalyst of different core/shell system in the application of photocatalytic $H_2$- production.

## References

1. Yun, H. J. *et al.* A Combination of Two Visible-Light Responsive Photocatalysts for Achieving the Z-Scheme in the Solid State. *ACS Nano* **5**, 4084–4090 (2011).
2. Iwashina, K., Iwase, A., Ng, Y. H., Amal, R. & Kudo, A. Z Schematic Water Splitting into $H_2$ and $O_2$ Using Metal Sulfide as a Hydrogen-Evolving Photocatalyst and Reduced Graphene Oxide as a Solid-State Electron Mediator. *J. Am. Chem. Soc.* **137**, 604–607 (2015).
3. Iwashina, K. & Kudo, A. Rh-Doped SrTiO3 Photocatalyst Electrode Showing Cathodic Photocurrent for Water Splitting under Visible-Light Irradiation. *J. Am. Chem. Soc.* **133**, 13272–13275 (2011).
4. Guo, S. H., Li, X. H., Zhu, J. M., Tong, T. T. & Wei, B. Q. Au NPs@$MoS_2$ Submicron Sphere-ZnO Nanorod Hybrid Structures for Efficient Photocatalytic Hydrogen Evolution with Excellent Stability. *Small* **12**, 5692–5701 (2016).
5. Li, X. H. *et al.* Au Multimer@$MoS_2$ Hybrid Structures for Efficient Photocatalytical Hydrogen Production via Strongly Plasmonic Coupling Effect. *Nano Energy* **30**, 549–558 (2016).

6. Meng, C. H. *et al*. Improved Solar-Driven Photocatalytic Performance of Highly Crystalline Hydrogenated $TiO_2$ Nanofibers with Core-Shell Structure. *Scientific Reports* **7**, 41825 (2017).
7. Chen, D. J., Zou, L. L., Li, S. X. & Zheng, F. Y. Nanospherical like reduced graphene oxide decorated $TiO_2$ nanoparticles: an advanced catalyst for the hydrogen evolution reaction. *Scientific Reports* **6**, 20335 (2016).
8. Wang, X., Li, Z., Shi, J. & Yu, Y. One-Dimensional Titanium Dioxide Nanomaterials: Nanowires, Nanorods, and Nanobelts. *Chem. Rev.* **114**, 9346–9384 (2014).
9. Yang, G. *et al*. A simple route to synthesize mesoporous titania from $TiOSO_4$: Influence of the synthesis conditions on the structural, pigments andphotocatalytic properties. *Appl. Surf. Sci.* **376**, 227–235 (2016).
10. Liao, G. Z., Chen, S., Quan, X., Chen, H. & Zhang, Y. B. Photonic Crystal Coupled $TiO_2$/Polymer Hybrid for Efficient Photocatalysis under Visible Light Irradiation. *Environ. Sci. Technol.* **44**, 3481–3485 (2010).
11. Antoniadou, M., Panagiotopoulou, P., Kondarides, D. I. & Lianos, P. Photocatalysis and photoelectrocatalysis using nanocrystalline titania alone or combined with Pt, $RuO_2$ or NiO co-catalysts. *J. Appl. Electrochem.* **42**, 737–743 (2012).
12. Liu, S., Yan, Y. H., Guan, W. W., Li, M. Z. & Jiang, R. Y. Role of nn Anatase-Rutile Heterojunction in the Photocatalysis of Mixed-Phase Titania. *Asian J. Chem.* **25**, 1307–1310 (2013).
13. Pan, L. *et al*. $TiO_2$ rutile–anatase core-shell nanorod and nanotube arrays for photocatalytic applications. *RSC Adv.* **3**, 3566–3571 (2013).
14. Qiu, Y. & Ouyang, F. Fabrication of $TiO_2$ hierarchical architecture assembled by nanowires with anatase/$TiO_2$(B) phase-junctions for efficient photocatalytic hydrogen production. *Appl. Surf. Sci.* **403**, 691–698 (2017).
15. Li, W. *et al*. Enhanced Photocatalytic Activity in Anatase/$TiO_2$(B) Core-Shell Nanofiber. *J. Phys. Chem. C* **112**, 20539–20545 (2008).
16. Cai, J. M. *et al*. *In Situ* Formation of Disorder-Engineered $TiO_2$(B)-Anatase Heterophase Junction for Enhanced Photocatalytic Hydrogen Evolution. *ACS Appl. Mater. Interfaces* **7**, 24987–24992 (2015).
17. Bai, S. *et al*. Boosting Photocatalytic Water Splitting: Interfacial Charge Polarization in Atomically Controlled Core-shell Co-catalyst. *Angew. Chem. Int. Ed.* **54**, 14810–14814 (2015).
18. Zhang, Q. *et al*. Effect of redox cocatalysts location on photocatalytic overall water splitting over cubic $NaTaO_3$ semiconductor crystals exposed with equivalent facets. *ACS Catal.* **6**, 2182–2191 (2016).
19. Bai, S. *et al*. A unique semiconductor-metal-graphene stack design to harness charge flow for photocatalysis. *Adv. Mater.* **26**, 5689–5695 (2014).
20. Xu, D. F., Hai, Y., Zhang, X. C., Zhang, S. Y. & He, R. A. $Bi_2O_3$ cocatalyst improving photocatalytic hydrogen evolution performance of $TiO_2$. *Appl. Surf. Sci.* **400**, 530–536 (2017).
21. Ma, Y. *et al*. Titanium dioxide-based nanomaterials for photocatalytic fuel generations. *Chem. Rev.* **114**, 9987–10043 (2014).
22. Antony, R. P. *et al*. Efficient photocatalytic hydrogen generation by Pt modified $TiO_2$ nanotubes fabricated by rapid breakdown anodization. *Int. J. Hydrogen Energy* **37**, 8268–8276 (2012).
23. Sreethawong, T. & Yoshikawa, S. Impact of photochemically deposited monometallic Pt and bimetallic Pt-Au nanoparticles on photocatalytic dye-sensitized H2 production activity of mesoporous-assembled $TiO_2$-$SiO_2$ mixed oxide nanocrystal. *Chem. Eng. J.* **197**, 272–282 (2012).
24. Kim, J. W., Monllor-Satoca, D. & Choi, W. Y. Simultaneous production of hydrogen with the degradation of organic pollutants using $TiO_2$ photocatalyst modified with dual surface components. *Energy Environ. Sci.* **5**, 7647–7656 (2012).
25. Chiarello, G. L., Aguirre, M. H. & Selli, E. Hydrogen production by photocatalytic steam reforming of methanol on noble metal-modified $TiO_2$. *J. Catal.* **273**, 182–190 (2010).
26. Xiang, Q. J., Yu, J. G. & Jaroniec, M. Synergetic effect of $MoS_2$ and graphene as cocatalysts for enhanced photocatalytic $H_2$ production activity of $TiO_2$ nanoparticles. *J. Am. Chem. Soc.* **134**, 6575–6578 (2012).
27. Yu, J. G. & Ran, J. R. Facile preparation and enhanced photocatalytic $H_2$-production activity of $Cu(OH)_2$ cluster modified $TiO_2$. *Energy Environ. Sci.* **4**, 1364–1371 (2011).
28. Zhang, L., Tian, B., Chen, F. & Zhang, J. Nickel sulfide as co-catalyst on nanostructured $TiO_2$ for photocatalytic hydrogen evolution. *Int. J. Hydrogen Energy* **37**, 17060–17067 (2012).
29. Chen, C. J., Liao, C. H., Hsu, K. C., Wu, Y. T. & Wu, J. C. P-N junction mechanism on improved NiO/$TiO_2$ photocatalyst. *Catal. Commun.* **12**, 1307–1310 (2011).
30. Tian, J., Liu, Q., Asiri, A. M. & Sun, X. Self-supported nanoporous cobalt phosphide nanowire arrays: an efficient 3D hydrogen-evolving cathode over the wide range of pH 0-14. *J. Am. Chem. Soc.* **136**, 7587–7590 (2014).
31. Liang, Y., Liu, Q., Asiri, A. M., Sun, X. & Luo, Y. Self-supported FeP nanorod arrays: a cost-effective 3D hydrogen evolution cathode with high catalytic activity. *ACS Catal.* **4**, 4065–4069 (2014).
32. Xiao, P. *et al*. Molybdenum phosphide as an efficient electrocatalyst for the hydrogen evolution reaction. *Energy Environ. Sci.* **7**, 2624–1629 (2014).
33. Cao, S., Chen, Y., Hou, C. C., Lv, X. J. & Fu, W. F. Cobalt phosphide as a highly active non-precious metal cocatalyst for photocatalytic hydrogen production under visible light irradiation. *J. Mater. Chem. A* **3**, 6096–6101 (2015).
34. Cao, S., Chen, Y., Wang, C. J., Lv, X. J. & Fu, W. F. Spectacular photocatalytic hydrogen evolution using metal-phosphide/CdS hybrid catalysts under sunlight irradiation. *Chem. Commun.* **51**, 8708–8711 (2015).
35. Yang, D. J. *et al*. An efficient photocatalyst structure: $TiO_2$(B) nanofibers with a shell of anatase nanocrystals. *J. Am. Chem. Soc.* **131**, 17885–17893 (2009).
36. Hara, M., Nunoshige, J., Takata, T., Kondo, J. N. & Domen, K. Unusual enhancement of $H_2$ evolution by Ru on TaON photocatalyst under visible light irradiation. *Chem. Commun.* **24**, 3000–3001 (2003).
37. Lin, C. H., Chao, J. H., Liu, C. H., Chang, J. C. & Wang, F. C. Effect of calcination temperature on the structure of a Pt/$TiO_2$(B) nanofiber and its photocatalytic activity in generating $H_2$. *Langmuir* **24**, 9907–9915 (2008).
38. Zhang, J., Qi, L., Ran, J., Yu, J. & Qiao, S. Z. Ternary NiS/$Zn_xCd_{1-x}S$/Reduced Graphene Oxide Nanocomposites for Enhanced Solar Photocatalytic $H_2$-Production Activity. *Adv. Energy Mater.* **4**, 1301925–1301931 (2014).
39. Zhang, W., Wang, Y., Wang, Z., Zhong, Z. & Xu, R. Highly efficient and noble metal-free NiS/CdS photocatalysts for $H_2$ evolution from lactic acid sacrificial solution under visible light. *Chem. Commun.* **46**, 7631–7633 (2010).
40. Yu, J. G., Hai, Y. & Cheng, B. Enhanced photocatalytic $H_2$-production activity of $TiO_2$ by Ni $(OH)_2$ cluster modification. *J. Phys. Chem. C* **115**, 4953–4958 (2011).
41. Tran, P. D. *et al*. Enhancing the photocatalytic efficiency of $TiO_2$ nanopowders for $H_2$ production by using non-noble transition metal co-catalysts. *Phys. Chem. Chem. Phys.* **14**, 11596–11599 (2012).
42. Tian, J. *et al*. Enhanced photocatalytic performances of $CeO_2$/$TiO_2$ nanobelt heterostructures. *Small* **9**, 3864–3872 (2013).
43. Zhang, X., Zhang, L., Xie, T. & Wang, D. Low-temperature synthesis and high visible-light-induced photocatalytic activity of BiOI/$TiO_2$ heterostructures. *J. Phys. Chem. C* **113**, 7371–7378 (2009).
44. Yang, G. *et al*. Well-Designed 3D $ZnIn_2S_4$ nanosheets$TiO_2$ nanobelts as Direct Z-Scheme photocatalysts for $CO_2$ Photoreduction into Renewable Hydrocarbon Fuel with High Efficiency. *Appl. Catal. B: Environ.* **219**, 611–618 (2017).


## Acknowledgements

This work is supported by the National Natural Science Foundations of China (Grant No.21577132), the Fundamental Research Funds for the Central Universities (Grant No. 2652015225).

## Author Contributions

G. Yang, H. Ding and D.M. Chen designed the main study. Jiejie Feng, Qiang Hao and Sijia Sun take part in the experiments. W.H. Ao analyzed the data. All authors reviewed the manuscript.

## Additional Information

**Supplementary information** accompanies this paper at https://doi.org/10.1038/s41598-017-15134-w.

**Competing Interests:** The authors declare that they have no competing interests.

**Publisher's note:** Springer Nature remains neutral with regard to jurisdictional claims in published maps and institutional affiliations.